

An Analytical Loading Model for n -Tendon Continuum Robots

Mohsen Moradi Dalvand , *Member, IEEE*, Saeid Nahavandi, *Senior Member, IEEE*,
and Robert D. Howe, *Fellow, IEEE*

Abstract—One of the key design parameters in tendon-driven continuum robots is the number of tendons and the tendon loading distribution. A load model is also helpful for avoiding slack in tendons that causes control inefficiency and inaccuracy. A quasi-static model of n -tendon continuum robots is derived using the Euler–Lagrange formulation. The model is employed to derive an analytical loading model for equidistant tendon tensions for any given beam configuration within the workspace. The model accounts for the bending and axial compliance of the manipulator as well as tendon compliance. Features of the proposed model are discussed and some of the potential applications are explained. Based on the proposed model, a slack avoidance algorithm with analytical formulation is developed to dynamically optimize the tendon loads while preventing slack in tendons for a given configuration. The proposed model is experimentally validated in a multitendon continuum robot system for four case studies of three- to six-tendon arrangements in open-loop control architecture. A stereo vision-based three-dimensional reconstruction system measures the beam configuration and properties for each of the three- to six-tendon continuum robots. The effect of number of tendons on the tension loads in n -tendon continuum robots is studied. A quantitative dimensionless relationship between the number of tendons, the maximum tendon loads, and the bending angles is developed that may be used as a design tool for tradeoff among the complexity and required force and size.

Index Terms—Analytical model, catheter, continuum robot, flexible manipulator, kinematics, load distribution, robotic surgery, slack avoidance, snake robot, statics, tendon-driven manipulator.

I. INTRODUCTION

CONTINUUM robots are found in a variety of fields, from industrial inspection to medical procedures, where there is a requirement for navigating through complex and constrained environments [1]–[6]. They are inspired by natural continuum

Manuscript received March 7, 2018; accepted April 20, 2018. This paper was recommended for publication by Associate Editor J. Paik and Editor I-M. Chen upon evaluation of the reviewers' comments. (*Corresponding author: Mohsen Moradi Dalvand.*)

M. M. Dalvand is with the Institute for Intelligent Systems Research and Innovation, Deakin University, Geelong, VIC 3216 Australia, and also with the Harvard School of Engineering and Applied Sciences, Cambridge, MA 02138 USA (e-mail: mdalvand@seas.harvard.edu).

S. Nahavandi is with the Institute for Intelligent Systems Research and Innovation, Deakin University, Geelong, VIC 3216, Australia (e-mail: saeid.nahavandi@deakin.edu.au).

R. D. Howe is with the Harvard School of Engineering and Applied Sciences, Cambridge, MA 02138 USA (e-mail: howe@seas.harvard.edu).

Color versions of one or more of the figures in this paper are available online at <http://ieeexplore.ieee.org>.

Digital Object Identifier 10.1109/TRO.2018.2838548

structures such as elephant trunks [7], octopus arms [8], squid tentacles [9], and snakes [10], [11]. In the medical field, catheters and catheter-like instruments are well-known examples of continuum structures that have gained attention in minimally invasive treatments [12], [13]. The continuous structure and inherent compliance of catheters enable them to exhibit elastic deformation along their entire length and navigate safely through tissues [14]. Instead of being defined by a finite set of joint parameters, they are more accurately defined with spatial curves [15]. This introduces more complexity in shape and position control of these systems as opposed to rigid link structures [16]–[18].

Tendon-driven mechanisms are well-known actuation systems for continuum robots and catheters [19]. Kinematics analysis is used to determine the tendon displacements for a given configuration in the workspace [4], [5], [18], [20], [21]. However, tendons can only support tension (negative load) and in compression they tend to buckle (go slack) because of their low bending stiffness [20], [22]. Actuation of a slacked tendon will first recover the slack before producing tension in the tendon [23]. This latency results in actuator backlash that is one of the key causes of inefficiency and inaccuracy in the controllers of robotic catheters [24]. Slack in redundant tendon-driven systems may or may not cause tip position inaccuracy; however, it directly affects the stiffness of the articulating beam and also the load distribution among tendons [13]. Approaches to prevent slack while minimizing tendon loading were studied in redundant rigid-link tendon-driven mechanisms [25]–[28]. Slack may be removed by applying more loads in tendons. High tendon load in continuum robots generates less compliance and more friction. Therefore, slack and excessive loads are both undesirable characteristics especially in catheters in which tendon size and materials are constrained by the environment [13], [29].

The tension in tendons will cause compression and bending in the compliant manipulator and extension in the tendons. This produces a coupled mechanical and kinematics problem that requires a loading model to address both of these aspects. This model has immediate applications not only in design process, to determine the required power for the actuators based on the mechanical properties of the continuum structure and tendons, but also in control algorithm in order to avoid slack (positive load) as well as excessive loading for any given configuration in workspace. This model is also useful for determining the tendon extension to increase position accuracy especially in case of open-loop control solutions. Furthermore, establishing a relationship between the displacement and tension in tendons may

simplify the controller and improve performance and accuracy without using force sensors.

Several studies were reported on the distribution of internal/external loadings in planar and spatial pneumatic- and cable-driven continuum manipulators [16], [30]–[36]. Tension loads were estimated in a single segment three-tendon continuum robot with only two active tendons [37]. A mechanics-based model was proposed to numerically estimate the tendon loads in n -tendon planar continuum robots [23]. This work was later extended for spatial multitendon continuum robots [18]. In these studies, numerical optimization techniques were employed to estimate tendon tensions for continuum robots with more than three tendons. The model was experimentally validated only for a four-tendon continuum robot. Compared to this previous work, the model proposed here has the advantages of analytical representation, which can be directly employed to develop features and control algorithms including closed-form Jacobian matrix, inverse and forward kinematics, and slack avoidance control algorithm.

Another model for the statics and dynamics of robots with general tendon routing paths were also derived by coupling the classical Cosserat-rod and Cosserat-string models [35]. The main focus of this paper was on position control and accuracy in continuum robots with general tendon routing and external loading. However, although it is not included in this paper and there is no experimental result provided for tendon tension, theoretically speaking, the model may be used with numerical solution techniques to estimate tendon tensions in multitendon continuum robots. These studies do not promise a loading model capable of determining the tension in n -tendon continuum robot for a given configuration within workspace.

The main contribution of this study is the development of an analytical loading model for continuum robots with n equidistant tendons that, for a given robot configuration within the workspace, determines the unique tendon tensions. These tensions correspond to the tendon displacements obtained from inverse kinematics solution for the given configuration. The model accounts for bending and axial deformation of the continuum structure as well as the axial deformation of the tendons. In addition, an algorithm is also proposed to optimize the tendon tensions while it guarantees no slack in tendons for a given configuration. Experimental validations for three- to six-tendon robot configurations are also conducted to evaluate the proposed model. The model is further employed to study the effects of tendon count in n -tendon continuum robots. To the best knowledge of the authors, the proposed loading model, slack avoidance algorithm, and quantitative dimensionless effects of tendon counts have not been studied before in the literature.

In the following section, the model parameters are described. Based on the Lagrangian formalism, the quasi-static model of the n -tendon continuum robots is derived in Section II. Tendon load distribution in cases of one- and two-tendon robots are studied and a mechanical-based approach is proposed to derive the loading model for continuum robots with four or more tendons in Section III. Some potential applications of the proposed analytical model including slack avoidance, accounting for tendon elasticity, and using the Jacobian are discussed

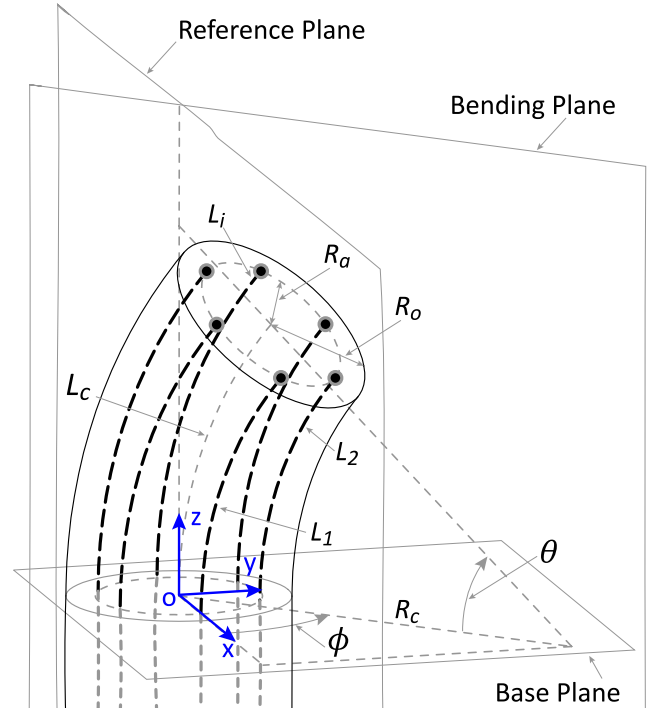


Fig. 1. Schematic description of the articulating beam of a tendon-driven catheter with n equidistant tendons ($n=6$ in this description) at a beam configuration (θ , ϕ , and L_c).

in Section IV. Section V provides details about experimental setup, procedure, and results. Effects of tendon counts are studied in IV-D followed by discussion and concluding remarks in Section VI.

II. QUASI-STATIC MODEL

A. Model Description

The assumptions involved in this study include the following.

- 1) The friction between the tendons and the tendons guides is zero [23], [35], [38].
- 2) The tendons always run parallel to the centroidal axis of the beam on a radially symmetric pattern at a fixed radius from the center of the beam [21], [23].
- 3) Compared to the elastic deformation energy, gravity, and inertial effects are negligible [18], [37].
- 4) The robot is under quasi-static equilibrium [39].

In the absence of external loading and disturbance, a set of material assumptions leading to linear elastic bending, linear axial deflections, and constant curvature are also exploited in the model [20], [40], [41].

Fig. 1 shows the schematic description of the articulating beam of a single segment cable-driven continuum robot with n tendons ($n=6$ in this case) in an arbitrary configuration. O_{xyz} is the reference Cartesian coordinate origin positioned at the base of the beam. Bending and bending plane angles of the beam are denoted by θ and ϕ . The length of the beam along its centerline is denoted by L_c . The length of the tendons from the termination point at the end of the beam to the base section of the beam is denoted by L_i ($i=1, \dots, n$). The bending radius

of the centerline of the beam is R_c . The tendons are embedded in the beam parallel to the centerline on a radially symmetric pattern at a radius of R_a from the center of the beam and evenly separated by angles of $\frac{2\pi}{n}$. Therefore, the tendons are equidistant from the beam centerline and from each other. For ease of illustration, the tendons are presented as infinitesimally thin tension elements. Considering the constant curvature assumption, the configuration states of the continuum structure are defined as θ , ϕ , and L_c . The actuator and task spaces of the continuum robots contain the tendon lengths and the pose information of the tip in the reference coordinate frame, respectively.

B. Model Derivation

In this section, a quasi-static load model for n -tendon continuum robots is derived. Based on the Euler–Lagrange equations for the general coordinates q , the quasi-static model of a continuum robot can be derived as

$$\frac{\partial V}{\partial q_i} = Q_i \quad i = 1, 2, 3 \quad (1)$$

where V is the potential energy and Q_i is generalized force for the coordinates $q = [\theta \ \phi \ L_c]^T$.

1) *Potential Energy*: Neglecting the gravity, the potential energy of the cable-driven continuum robots consists of the bending energy (V_b) and axial compression energy (V_a) in the beam as well as the extension potential energy in tendons (V_t). The potential energy of the articulating beam due to bending can be defined using Euler–Bernoulli beam element analysis as [42]

$$V_b = \frac{1}{2} EI \int_0^{L_0} \left(\frac{d\theta_p}{ds} \right)^2 ds = \frac{1}{2} \frac{EI}{L_0} \theta^2 \quad (2)$$

where E , I , and θ_p are the Young's modulus, area moment of inertia of the beam and bending angle of any point p along the length of the beam, respectively. Based on the constant curvature assumption, θ_p is equal to $s(\frac{\theta}{L_0})$ where s is the distance of the point p to the base along the centerline of the beam (arc length). The potential energy due to the axial compression of the beam [42] can be derived by

$$V_a = \frac{1}{2} EA \int_0^{L_0} \left(\frac{du_p}{ds} \right)^2 ds = \frac{1}{2} \frac{EA}{L_0} (L_c - L_0)^2 \quad (3)$$

where A and u_p are the cross section area of the beam and the axial compression of any point p along the length of the beam, respectively. Assuming the linear elastic beam, u_p is derived as $s(\frac{L_c - L_0}{L_0})$. Based on the same theory, the extension potential energies of the n tendons are

$$\begin{aligned} V_t &= \frac{1}{2} E_t A_t \sum_{i=0}^n \int_0^{L_{t_0}} \left(\frac{du_{t_p}}{ds_t} \right)^2 ds_t \\ &= \frac{1}{2} \frac{E_t A_t}{L_{t_0}} \sum_{i=0}^n (L_{t_i} - L_{t_0})^2 \end{aligned} \quad (4)$$

where A_t , E_t , and u_{t_p} are the cross section area, the Young's modulus of the tendons and the axial compression of any point p_t along the length of the tendon from the actuation to the

terminations points, respectively. Assuming the linear elastic tendon, $u_{t_p} = s_t \left(\frac{L_{t_i} - L_{t_0}}{L_{t_0}} \right)$ where L_{t_0} is the initial length of the tendons and s_t is the distance of the point p_t on tendon to the base along the centerline of the tendon (arc length).

2) *Generalized Force*: Generalized forces are the forces or torques acting on the generalized coordinates $[(\theta \ \phi \ L_c)^T]$ [43]. The three generalized forces in n -tendon continuum robots can be expressed as

$$\begin{cases} Q_\theta = \sum_{i=1}^n \left(F_i \frac{\partial L_{a_i}}{\partial \theta} \right) \\ Q_\phi = \sum_{i=1}^n \left(F_i \frac{\partial L_{a_i}}{\partial \phi} \right) \\ Q_{L_c} = \sum_{i=1}^n \left(F_i \frac{\partial L_{a_i}}{\partial L_c} \right) \end{cases} \quad (5)$$

where L_{a_i} is the actuator displacements and can be derived as

$$L_{a_i} = L_0 - L_c + R_a \theta \cos(\alpha_i) + \delta_i \quad i = 1, \dots, n \quad (6)$$

where L_0 is the initial length of the beam at rest, δ_i is the tendon extension due to the axial loading from the actuation to the termination points, and α_i is defined as

$$\alpha_i = \phi - 2\pi \frac{i-1}{n} \quad i = 1, \dots, n \quad (7)$$

Using (5) and (6), the generalized forces can be represented as

$$\begin{cases} Q_\theta = R_a \sum_{i=1}^n (F_i \cos(\alpha_i)) \\ Q_\phi = R_a \theta \sum_{i=1}^n (-F_i \sin(\alpha_i)) \\ Q_{L_c} = \sum_{i=1}^n (F_i) \end{cases} \quad (8)$$

Substituting (2)–(4) and (8) into the (1), the quasi-static model of an n -tendon continuum robot may be represented as

$$\frac{EI}{L_0} \theta = Q_\theta \quad (9a)$$

$$0 = Q_\phi \quad (9b)$$

$$\frac{EA}{L_0} (L_c - L_0) = Q_{L_c} \quad (9c)$$

for the three DOFs of θ , ϕ , and L_c , respectively. This constitutive equation captures the relationship between the mechanical response of beam strain (or configuration) and the tension load in tendons under quasi-static equilibrium condition. It should be noted that this equation is independent of the actuator displacements and tendon extension. This static model matches the constitutive equation derived based on the beam mechanics in matrix form [18], [23]. Although there is no necessity in using the Euler–Lagrange formalism for development of the static model, it is more expandable and can be used to also develop the dynamic model of the continuum robots in future works.

III. LOAD ANALYSIS

To facilitate the development of the load model for general n -tendon robot, the proposed quasi-static model is employed to study the tendon load distribution for the general case of three or more tendon robots as well as special cases of one- or two-tendon robots in this section.

A. General Case—Three or More Tendons ($n \geq 3$)

If there are three actuated tendons ($n = 3$) in a continuum robot, it has three DOFs of θ , ϕ , and L_c that can be independently controlled, which results in a fully determined system. In this case, the tendon tension loads can be directly derived using (9) as functions of beam configuration parameters as

$$F_i = \frac{EA}{3L_0}(L_c - L_0) - \frac{2EI}{3L_0R_a}\theta \cos(\alpha_i) \quad (10)$$

$$i = 1, \dots, 3.$$

Having four or more tendons in a continuum robot makes the system overactuated and mathematically underdetermined (three equations and four or more variables). Optimization techniques have been employed to numerically estimate the tendon tensions based on a weight function to satisfy optimization criteria, which may result in slack tendons and nonoptimal load distribution [18], [23]. Here, a mechanics-based approach is proposed to derive a tension loading model for n -tendon continuum robots for any possible beam configuration.

In a tendon driven continuum robot at the given beam configuration, the tension loads in the tendons correspond to both bending and axial compression of the articulating beam. The portion of the tension load in the i th tendon corresponding to the beam bending has direct linear relation to both the bending angle θ and the moment arm $R_a \cos(\alpha_i)$. Therefore, it may be expressed as $K_b R_a \theta \cos(\alpha_i)$, where K_b is a variable. The other portion of tension load in i th tendon that corresponds to the axial compression of the beam is directly related to the changes in the length of the beam ($L_c - L_0$). Thus, it can be represented by $K_a(L_c - L_0)$ with K_a being a variable. So the tension load applied to the i th tendon can be subsequently expressed as

$$F_i = K_a(L_c - L_0) + K_b R_a \theta \cos(\alpha_i) \quad (11)$$

$$\begin{cases} i = 1, \dots, n \\ n \geq 4. \end{cases}$$

By this definition, the resulting tensions will be proportional to the displacements in the corresponding tendons that makes the tendons carry the local loads. This loading distribution is similar to the distribution that exists in one-, two-, and three-tendon cases as described in (15), (17), and (10). In other words, this definition will extend the loading distribution of one-, two-, and three-tendon cases to four and more tendons cases. By substituting (11) into (9a) and (9c), parameters K_a and K_b can be determined as

$$K_a = \frac{AE}{nL_0} \quad (12)$$

$$K_b = -\frac{2EI}{nL_0R_a^2}.$$

As implied by (12), parameters K_a and K_b are functions of the geometry and mechanical property of the articulating beam and the fixed locations of the tendons. The tension load applied to the i th tendon (F_i) in a continuum robot with four or more tendons can be derived by substituting K_a and K_b back into the (11). The loading model derived in (11) also works for three-tendon

robots and, for $n = 3$, it results in (10). Equations (15), (17), and (11) can be used to determine the tendon tension loads in robots with one, two, and three or more tendons, respectively. In order to provide a single formula for n tendons ($n \geq 1$), a parameter k is introduced that represents the number of controllable DOFs of the robot. With this introduction, these equations may be combined into a single equation

$$F_i = \frac{E}{L_0R_a n} (AR_a(L_c - L_0) - (k - 1)I\theta \cos(\alpha_i)) \quad (13)$$

$$i = 1, \dots, n$$

where k is defined as

$$k = \begin{cases} n & \text{if } n = 1, 2 \\ 3 & \text{if } n \geq 3. \end{cases} \quad (14)$$

This load distribution formulation determines the tendon tensions in a robot with any number of tendons ($n \geq 1$) for any given configuration within the workspace. It should be noted that this proposed load distribution makes each tendon tension proportional to the tension displacement obtained from the inverse kinematics solution (6) for the given configuration.

B. Special Cases—One- or Two-Tendon ($n < 3$)

If there is only single actuated tendon in a robot, it has only one DOF; either θ or L_c , and ϕ is zero. In this case, either of (9a) or (9c) can be utilized to derive the tendon tension load as a function of the beam configuration as

$$F_1 = -\frac{EI\theta}{L_0R_a} = \frac{AE(L_c - L_0)}{L_0}. \quad (15)$$

Alternatively, (13) may be used with $n = 1$ and $k = 1$ to obtain similar representation of the tension load in single-tendon robot as presented in (15). In case of a single-tendon catheter, the variables θ and L_c are dependent and their relationship may be presented as

$$L_c = L_0 - \frac{I}{AR_a}\theta. \quad (16)$$

If there are two actuated tendons in a robot separated by 180° angle, the mechanical system becomes a system with two DOFs of θ and L_c . ϕ is still not controllable and is either zero or 180° . Entering $n = 2$ and $k = 2$ in (13) results in the tendon tension load in i th tendon in two-tendon robot configuration as

$$F_i = \frac{1}{2} \frac{EA}{L_0}(L_c - L_0) - \frac{1}{2} j \frac{EI}{L_0R_a}\theta \quad (17)$$

$$j = \begin{cases} 1 & \text{if } i = 1 \\ -1 & \text{if } i = 2. \end{cases}$$

Alternatively, both (9a) and (9c) may be utilized to derive the tension loads in two-tendon robot as a function of beam configuration as presented in (17).

C. Load Distribution

The constitutive equation (9) for continuum robots with four or more tendons is underdetermined. It includes $(n - 3)$ free

variables that may be chosen based on the desired behavior of the system and the three remaining variables need to be determined using the constitutive equation to satisfy equilibrium. This arbitrary selection of tensions for some of the tendons is mathematically meaningful; however, it is not physically relevant. This is because for a given beam configuration, there is a unique set of tendon tensions corresponding to the tendon displacements determined by the inverse kinematics solution for the given configuration. This means that if, based on the inverse kinematics solution for a given configuration, a set of tendon displacements is commanded to the continuum robot, the resulting tendon tensions are unique. The beam structure distributes the loads among all the tendons based on their locations if the tendon displacements correspond to the given configuration. This is reflected in the proposed model as it produces a unique set of tensions for any given configuration within the workspace. Therefore, one advantage of the proposed model is to provide a simple closed-form expression for tendon tensions that can be used to, for example, avoid slack, which makes the control easy to perform in position space.

On the other hand, in a force control scenario, a set of tendon tensions may be chosen, i.e., the tendon tension(s) as free variable(s) can be chosen arbitrarily based on the desired performance and the three remaining tension variables need to be obtained using the constitutive equation, to serve as input commands that moves the robot to the same beam configuration. However, it does not result in same tendon displacements and stretches as those determined by the inverse kinematics solution for similar configuration. In this case, the arbitrary selection of tendon tensions is both mathematically meaningful and physically relevant. It may be possible to adjust the tension loads based on the desired behavior, for example, to lower the peak tensions; however, this would require continuous supervision and numerical optimization algorithms for control and slack avoidance in the system.

To further study the load model proposed in (13), two tendons are randomly chosen and the relationship between their tensions for a given configuration is investigated. Load distribution in n -tendon continuum robots ($n = 6$ in this example) for a given configuration (θ , ϕ , and L_c) is schematically described in Fig. 2. Two arbitrary tendons i and j are selected and their tension vectors are illustrated in this figure by F_i and F_j that represent the magnitude and direction of these tension loads. End points of these tension vectors belong to the line $p_x p_y$. The slope of this line in $O_{t_{xy}}$ coordinates lying on the bending plane with its origin located at the tip of the robot (see Fig. 2) is

$$m = \frac{F_i - F_j}{R_{ij}} \quad (18)$$

where R_{ij} is defined as

$$R_{ij} = R_a \cos(\alpha_i - \phi) - R_a \cos(\alpha_j - \phi) \quad \begin{cases} i, j = 1, \dots, n \\ i \neq j. \end{cases} \quad (19)$$

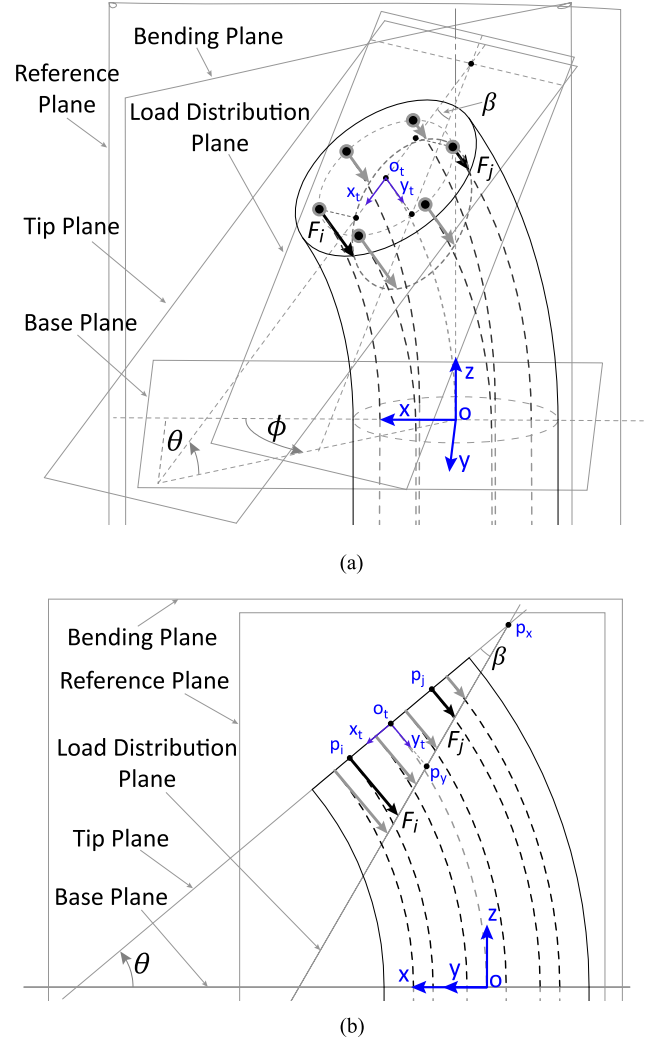


Fig. 2. Schematic description of load distribution in n -tendon continuum robots ($n = 6$ in this example) at a given configuration (θ , ϕ , and L_c). (a) 3-D isometric view. (b) Projected view on the bending plane.

Substituting (13) and (19) into (18) yields the slope of the line $p_x p_y$ as

$$m = \frac{2EI\theta}{nL_o R_a^2}. \quad (20)$$

The x - and y -intercepts of this line are

$$b_x = \frac{AR_a^2(L_o - L_c)}{2I\theta} \quad (21)$$

$$b_y = \frac{AE(L_o - L_c)}{nL_o}. \quad (22)$$

From (20) and (22), the slope and y -intercept of the line $p_x p_y$ are not dependent on the location of the i th or j th tendons and are functions of beam properties, tendon count, and beam configuration. This reveals the linearity feature of the loading distribution among tendons for n -tendon continuum robots for any given beam configuration within workspace, as illustrated in Fig. 2. It should be noted that linear loading distribution is only

valid if tendons are equidistant from each others and centerline of the beam. The linearity property of the loading distribution in n -tendon continuum robots may be directly utilized, as an alternative method to the proposed mechanics-based solution described in Section III-A, to solve the underdetermined constitutive equation that results in a similar analytical formulation as presented in (13).

IV. MODEL APPLICATIONS

The analytical load model proposed in (13) may be used in control algorithms to increase efficiency and accuracy by, for example, avoiding slack in tendons, accounting for tendon elasticity, and providing a Jacobian matrix, as described in the following sections.

A. Slack Avoidance

The tendon tensions obtained from the load model presented in (13) correspond to the actuator displacements of (6), which may result in positive tensions or slack in tendons. This means that to reach a given beam configuration, the tendons would have to act like solid rods capable of pushing and pulling along their axis. A key benefit of the proposed tendon tension model is that it can facilitate development of analytical algorithm for avoiding slack in n -tendon continuum robots without need of any optimization or numerical methods [23]. The value of ϕ at which the maximum tension load in the i th tendon happens may be determined using (13) as

$$\phi_{F_{\max}} = 2\pi \frac{i-1}{n} + q\pi \begin{cases} i = 1, \dots, n \\ q \in 2\mathbb{N} + 1. \end{cases} \quad (23)$$

In order to avoid slack in tendons, the maximum tension load in any of the tendons in any bending plane angle ϕ should not be more than zero. This means that, to reach a desired θ and ϕ with no slack in the tendon with lowest tension and also with linear tendon loading distribution, the maximum beam length ($L_{c_{\max}}$) needs to be determined in a way that the beam configuration (θ , ϕ , and $L_{c_{\max}}$) results in no slack and zero tension in the tendon with lowest tension. Substituting (23) into (13), the required length of the articulating beam to prevent slack in the worst case of zero tension load in the tendon may be obtained as

$$L_{c_{\max}} = L_0 + (k-1) \frac{I\theta}{AR_a} \quad k \geq 2. \quad (24)$$

The constraint $k \geq 2$ in this equation is because slack is meaningless in case of single-tendon robot. With this equation, for any desired bending angle, the length of the beam is determined independently from the bending plane angle in order to satisfy the peak condition of zero tension in tendons obtained from (23). In other words, it determines the biggest possible length of the beam that produces no slack in tendons for any given beam configuration. This guarantees that the tendon tensions are never positive while it further avoids excessive loads in the tendons by zeroing the load in the tendon located at the back of the beam on the bending plane at which the peak force is occurring. It is worth noting that depending on the desired beam configuration, L_c may be further extended to decrease the loading distribution

in tendons while it still satisfies the no slack requirement. This is possible by manipulating the tension load at the location of the farthest tendon at the back rather than the tendon located at $\phi_{F_{\max}}$. This, however, produces a different loading distribution that is beyond the scope of this paper and will be presented and discussed in future work. Substituting (24) into the (13), the new tendon loading distribution model in an n -tendon robot guaranteeing no slack and optimizing tension loads is

$$F_{i_{\text{NoSlack}}} = \frac{EI\theta}{L_0 R_a n} (k-1) \times (1 - \cos(\alpha_i)) \quad k \geq 2 \\ i = 1, \dots, n. \quad (25)$$

It should be noted that this load model is not dependent on L_c . The reason is that for a given beam configuration (θ , ϕ , and L_c), the updated beam configuration (θ , ϕ , and $L_{c_{\max}}$) is used to develop this model where $L_{c_{\max}}$ is obtained from (24). In other words, the slack avoidance algorithm requires only the target bending angle θ to determine the longest length of the continuum structure guaranteeing both no slack and optimized loading in tendons.

B. Tendon Elasticity

The proposed analytical loading model may also be useful in increasing accuracy and performance of control algorithms by accounting for tendon elasticity. Based on Hook's law and the tension loads in tendons, the axial extension in tendons is

$$\delta_i = \frac{F_i L_{0i}}{E_t A_t} \quad i = 1, \dots, n \quad (26)$$

where E_t , A_t , and L_{0i} are the Young's modulus, cross section area, and initial length of the tendon at rest, respectively. This equation can be used in (6) to determine the actuator displacements.

C. Jacobian Matrix

One advantage of the proposed analytical approach is that it facilitates derivation of closed-form Jacobian, which may be useful in position control of a continuum robot based on the tendon tensions. This may be problematic for numerical optimization based approaches [23]. Based on the proposed loading model, the Jacobian matrix of the tendon tensions may be derived as function of beam configuration as

$$J_{F_i}(\theta, \phi, L_c) = \left[\frac{\partial F_i}{\partial(\theta, \phi, L_c)} \right]_{n \times 3} \\ = \frac{E}{nL_0} \left[\frac{-2I}{R_a} \cos(\alpha_i) \quad \frac{-2I}{R_a} \theta \sin(\alpha_i) A \right]_{n \times 3} \\ i = 1, \dots, n. \quad (27)$$

D. Effects of Tendon Count

In this section, the proposed model is used to study the effects of the number of tendons in continuum robots. The maximum tension load of the i th tendon in an n -tendon robot ($n \geq 2$) at the

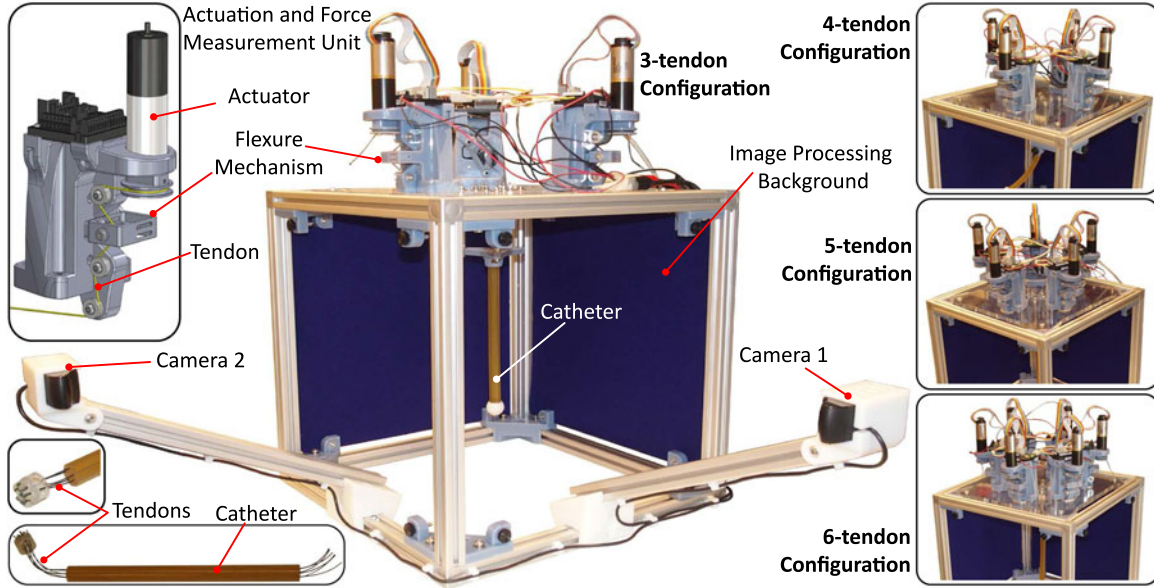


Fig. 3. Modular continuum robotic system capable of manipulating catheters with up to six tendons integrated with a real-time vision-based 3-D reconstruction system.

bending plane angle $\phi_{F_{\max}}$ (23) for any bending angle θ within the workspace of the robot can be derived using (13) as

$$F_{i_{\max}} = -\frac{2EI}{L_0 R_a} \left(\frac{k-1}{n} \right) \theta = C_F \gamma. \quad (28)$$

In this equation, the parameter $C_F = -\frac{2EI}{L_0 R_a}$ is a constant of geometry and mechanical properties of the articulating beam, and the variable $\gamma = \left(\frac{k-1}{n} \right) \theta$ is a dimensionless parameter. The parameter γ relates the bending angle and tendon count to the maximum tendon tension for the case of no slack in any of the tendons. Therefore, γ may be used to represent the effects of the tendon count on the tension loads in tendons. A contour plot illustrating of the variable γ is shown in Fig. 4 for the bending angles of 0° to 90° for robots with three and more tendons. γ is identical for the robots with two- and four-tendon. Therefore, to produce a continuous trend in the plot, the two-tendon case is not included in this plot. Based on the design parameters of tendon count and the maximum required bending angle for a specific application, the variable γ can be obtained using this plot. The maximum required tension loads in tendons can then be determined by multiplying the obtained γ by the constant C_F , which can be adjusted for the designated application.

Equation (28) represents a linear relationship between the maximum tendon loads and bending angle for any number of tendons. Therefore, as implied from the plot, the lower number of tendons causes more increase in maximum tendon loads as the bending angle increases. In other words, the more tendons, the lower the tension loads. Furthermore, as the number of tendons increases, the magnitude of the maximum tendon load decreases for the same amount of curvature (bending angle). On the other hand, there is a hyperbolic relationship between the tendon loads and number of tendons (proportional to $1/n$) at any bending angle. This plot can be utilized as a design tool representing the tradeoff between the number of tendons and the maximum

force of the actuators in an n -tendon continuum robot. This plot is applicable for any multitendon continuum robot independent of the size and material property of the continuum structure and tendons.

V. EXPERIMENTS

A. Experimental Setup

In order to evaluate the proposed model for tendon tension in n -tendon continuum robots (13), a catheter is commanded to a series of beam configurations in a multitendon catheter robot system in an open-loop control architecture. This system described in Fig. 3 is integrated with a real-time vision-based shape sensing system that enables the three-dimensional (3-D) reconstruction of the catheters at the rate of 200 Hz with the accuracy of ± 0.6 mm and $\pm 0.5^\circ$ for the linear and angular parameters, respectively, [15], [44]. This modular system is designed so that it can actuate catheters with up to six tendons. DC geared motors (Maxon Motors Inc. Model EC-max 22, Fall River, MA, United States) are utilized for the actuation of the tendons (see Fig. 3). Load-cells (Model FC22, Phidgets Inc., Calgary, AB, Canada) are incorporated into the actuation modules using a flexure mechanism enabling measurement of the tension loads in tendons. Load-cells are calibrated using known weights. To decrease the friction between the tendon and pulleys, low-friction pulleys with ball bearing are employed in the system.

Tendons used in this setup are Spectra microfilament braided lines (Spectra, PowerPro Inc., Irvine, CA, United States). The multilumen catheters were molded out of urethane rubber compounds (PMC 780, Smooth-On Inc., Macungie, PA, United States). The catheter bodies are 160 mm in length and 6 mm in radius with three- to six-lumen located at the radius of 3.5 mm from the centroid axis. The Young's modulus of the catheters

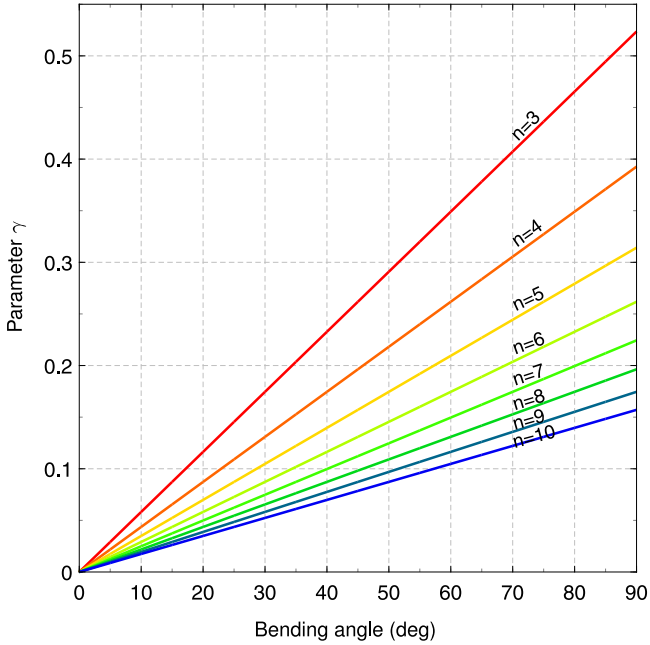


Fig. 4. Contour plot illustrating the quantitative relationship between the number of tendons (n) and the tendon tension loads with no slack in multitendon continuum robots as a function of bending angle, independent of the geometry and material property of the robot.

and tendons are measured using an Instron 5566 universal testing machine to be 5.9 MPa and 48.9 GPa, respectively. As shown in Fig. 3, tendons are passed through the lumens and knotted to the actuator spools from one end and to a 3-D printed part from the other end at termination point at distal end of the catheter. The system was operated by a PC with Intel Core i7 processors running at 3.00 GHz with 16 GB of memory.

B. Experiment Procedure and Results

For each of the three- to six-tendon catheters, the robot was commanded from its home configuration (at rest in vertical position with zero tension in tendons) as shown in Fig. 3 to bending angles of 10° , 30° , and 50° and bending plane angles of 0° , 45° , 90° , 135° , 180° , 225° , 270° , and 315° . The length of the catheter for each of the bending and bending plane angles was calculated from (24) to avoid slack and excessive loading in the tendons at target configuration. For each of the three- to six-tendon catheters, the calculated length of the catheter and the desired bending and bending plane angle were commanded to the robot and the trial was repeated three times; resulting in 288 trials in total. In the experiments, the measured tendon tension loads, bending and bending plane angle, and the length of the catheter obtained from the 3-D reconstruction algorithm [15] were recorded. The obtained beam configuration parameters served as input for (13) to estimate the tension loads in tendons. The results for the three repetitive trials were analyzed to evaluate the repeatability. An average 3% difference between the trials was measured, which shows high repeatability between the trials. Maximum 0.7 and 0.3 mm compression and extension were measured for the catheters and tendons, respectively,

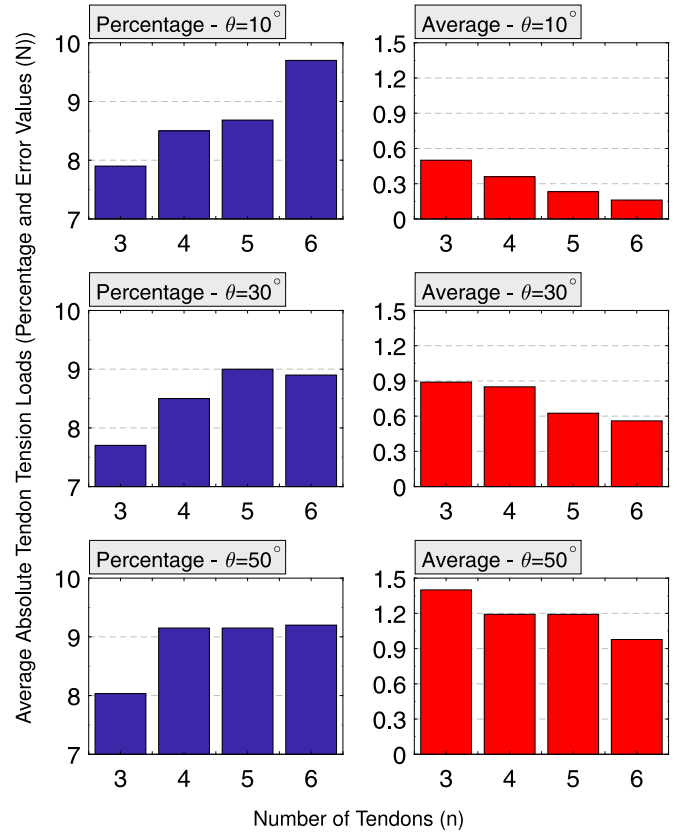


Fig. 5. Percentage (left column) and absolute values (right column) of the mean errors between the estimated and measured tension loads in the tendons of three- to six-tendon continuum robots for the bending angles of 10° , 30° , and 50° , respectively, from top to bottom (mean value of the three repetitive trials).

across all experiments. The percentage and the absolute values of the errors in the estimated tendon tension loads for all of experiments for each of the three- to six-tendon catheters are compiled in Fig. 5. The results are the mean values for the three repetitive trials for each of the three- to six-tendon catheters.

There is no significant difference between the percentage mean errors for the three bending angles. This is basically due to the fact that the magnitude of the loads increases as the bending angle increases causing similar percentage errors for different curvatures. On the other hand, as the bending angle increases, the average absolute error value increases in individual three- to six-tendon catheters. The average absolute error was increased by around 0.7 N at the highest bending angle compared to the lowest angle. This is also independent of the number of tendons (see Fig. 5). The error percentages of the estimated tendon loads increases as the number of tendon increases. This is opposed to the average absolute values of the errors, which is less in catheters with more tendons. This trend is independent of the bending angle of the configuration. The mean value and percentage error of all of the experiments for the three repetitive trials for the three bending angles and eight bending plane angles for all of the three- to six-tendon catheters are calculated to be 0.74 N and 8.61% of the maximum loads of each experiment.

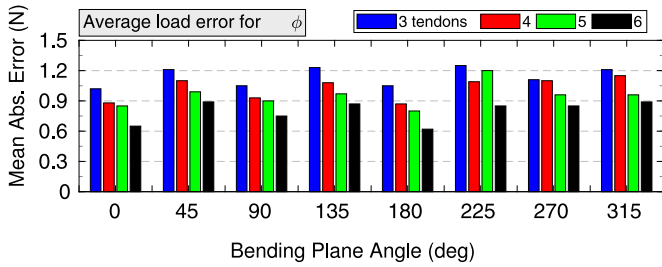


Fig. 6. Mean absolute errors between the estimated and measured tension loads in the tendons of three- to six-tendon continuum robots for different bending plane angles of 0° , 45° , 90° , 135° , 180° , 225° , 270° , and 315° , respectively (mean value of the three repetitive trials).

Fig. 6 presents the mean absolute errors in the estimated tendon tension loads for all of experiments for each of the three- to six-tendon catheters in different bending plane angles. There is no significant difference between the loads in different bending plane angles. However, similar to the loads compared based on the bending angle (see Fig. 5), the error decreases as the number of tendons decreases. This may be simply because having more tendons decreases the overall magnitude of the tension loads in tendons. Maximum and standard deviation errors between estimated and measured tendon tension loadings are 1.52 and 0.6 N across all experiments.

The absolute mean and maximum errors of 1.04° and 3.05° for the bending angle, 1.23° and 3.24° for the bending plane angle, and 0.67 and 1.21 mm for the length of the beam structure are measured between the commanded and measured beam configurations throughout the experiments. This demonstrates good position accuracy of the open-loop control of continuum robot based on the developed tension model. The mean percentages of the goodness of fit for the circles and ellipsis fitted to the continuum structure throughout the experiments are measured 99.61 and 99.86, respectively. This proves the validity of the constant curvature assumption exploited in the proposed model. The absolute maximum tension loads of the tendons located at the back of the continuum structure throughout the experiments are measured to be less than 0.1 N, which validates the accuracy and effectiveness of the proposed slack avoidance algorithm.

Given the fact that effects of gravity, friction, viscoelasticity, and nonlinearity in materials and mechanical system are neglected in the proposed model, the experimental results presented reasonable accuracy (91.3%) for the tension load model of the three- to six-tendon continuum robots. The errors are low for the small bending angles and increase for the larger bending angles, probably due to the friction between tendons and lumens [45]. Other causes include uncertainties in the properties of the beam and tendon material and measurement errors in the vision-based 3-D reconstruction system (± 0.6 mm and $\pm 0.5^\circ$). The locations of the tendons within the cross section of the articulating beam were assumed to be fixed during the deformation. However, for ease of fabrication, the lumens were manufactured with the diameter twice as big as the tendons. This leads to the tendons running not exactly parallel to the beam centerline and may cause some minor errors as well.

VI. CONCLUSION

In this paper, a quasi-static model for equidistant tendon tensions based on a linear distribution of tendon tensions in n -tendon continuum robots was developed that accounts for the bending and axial compliance of the manipulator as well as the tendon compliance. The analytical loading model takes a given beam configuration within the workspace and determines the unique tendon tensions with linear distribution. These tensions are proportional to the tendon displacements obtained from inverse kinematics solution for the given configuration. A slack avoidance algorithm was proposed to analytically determine the optimized beam configuration that not only decreases the tendon tensions but also guarantees no slack in tendons. The model was experimentally verified for three- to six-tendon robots for different configurations in an open-loop control architecture. The experimental results demonstrated that the proposed model can accurately predict the tendon tension loading of a multitendon continuum robot with axial stretch in its tendons. The results of the experiments showed mean error of 0.74 N or 8.61% of the maximum loads of each experiments for the proposed model compared to the actual measurements.

Features of the loading distribution resulted from the proposed model including uniqueness and linearity were discussed and some of the potential applications of the proposed model including avoiding slack in tendons, accounting for tendon elasticity, and using Jacobian matrix were derived. A quantitative relationship between the number of tendons, the maximum tendon loads and the bending angles was established. Based on this dimensionless model, lower loads are expected in continuum robots with more tendons for a given beam configuration. This quantitative model may be used as a design tool for the tradeoff among the complexity (number of actuators, sensors, and complicated controller), force (required actuator force), and size (actuator size and tendon diameter). The proposed loading model may be helpful for real-time control and estimation of shape, position, and external load direction and magnitude in continuum robots and catheters that may result in safer operation. Future work may exploit the advantages of the proposed closed-form Jacobian in position control of continuum robots based on the tendon tensions. External load estimation and error analysis of the n -tendon continuum robots considering friction, external loading, and general tendon positioning may also be addressed in future work.

REFERENCES

- [1] M. A. Armada, G. Granosik, M. G. Hansen, and J. Borenstein, "The OmniTread serpentine robot for industrial inspection and surveillance," *Ind. Robot. Int. J.*, vol. 32, no. 2, pp. 139–148, 2005.
- [2] A. Wolf *et al.*, "A mobile hyper redundant mechanism for search and rescue tasks," in *Proc. IEEE/RSJ Int. Conf. Intell. Robots Syst.*, 2003, vol. 3, pp. 2889–2895.
- [3] H. B. Gilbert, J. Neimat, and R. J. Webster, "Concentric tube robots as steerable needles: Achieving follow-the-leader deployment," *IEEE Trans. Robot.*, vol. 31, no. 2, pp. 246–258, Apr. 2015.
- [4] N. Simaan *et al.*, "Design and integration of a telerobotic system for minimally invasive surgery of the throat," *Int. J. Robot. Res.*, vol. 28, no. 9, pp. 1134–1153, 2009.
- [5] B. A. Jones and I. D. Walker, "Kinematics for multisection continuum robots," *IEEE Trans. Robot.*, vol. 22, no. 1, pp. 43–55, Feb. 2006.

- [6] Y.-J. Kim, S. Cheng, S. Kim, and K. Iagnemma, "A novel layer jamming mechanism with tunable stiffness capability for minimally invasive surgery," *IEEE Trans. Robot.*, vol. 29, no. 4, pp. 1031–1042, Aug. 2013.
- [7] R. Cieslak and A. Morecki, "Elephant trunk type elastic manipulator-a tool for bulk and liquid materials transportation," *Robotica*, vol. 17, no. 1, pp. 11–16, 1999.
- [8] I. D. Walker *et al.*, "Continuum robot arms inspired by cephalopods," *Proc. SPIE*, vol. 5804, pp. 303–314, 2005.
- [9] C. B. Cay and B. A. long handled, "The functional morphology of the musculature of squid (Loliginidae) arms and tentacles," *J. Morphol.*, vol. 172, pp. 179–192, 1982.
- [10] M. Tanaka and K. Tanaka, "Control of a snake robot for ascending and descending steps," *IEEE Trans. Robot.*, vol. 31, no. 2, pp. 511–520, Apr. 2015.
- [11] A. M. Andruska and K. S. Peterson, "Control of a snake-like robot in an elastically deformable channel," *IEEE/ASME Trans. Mechatron.*, vol. 13, no. 2, pp. 219–227, Apr. 2008.
- [12] C. Bergeles, A. H. Gosline, N. V. Vasilyev, P. J. Codd, P. J. del Nido, and P. E. Dupont, "Concentric tube robot design and optimization based on task and anatomical constraints," *IEEE Trans. Robot.*, vol. 31, no. 1, pp. 67–84, Feb. 2015.
- [13] Y.-J. Kim, S. Cheng, S. Kim, and K. Iagnemma, "A stiffness-adjustable hyperredundant manipulator using a variable neutral-line mechanism for minimally invasive surgery," *IEEE Trans. Robot.*, vol. 30, no. 2, pp. 382–395, Apr. 2014.
- [14] K.-W. Kwok *et al.*, "Dimensionality reduction in controlling articulated snake robot for endoscopy under dynamic active constraints," *IEEE Trans. Robot.*, vol. 29, no. 1, pp. 15–31, Feb. 2013.
- [15] M. M. Dalvand, S. Nahavandi, and R. D. Howe, "Fast vision-based catheter 3D reconstruction," *Phys. Med. Biol.*, vol. 61, no. 14, pp. 5128–5148, 2016.
- [16] W. S. Rone and P. Ben-Tzvi, "Continuum robot dynamics utilizing the principle of virtual power," *IEEE Trans., Robot.*, vol. 30, no. 1, pp. 275–287, Feb. 2014.
- [17] H. Rafii-Tari, C. J. Payne, and G.-Z. Yang, "Current and emerging robot-assisted endovascular catheterization technologies: A review," *Ann. Biomed. Eng.*, vol. 42, no. 4, pp. 697–715, 2014.
- [18] D. B. Camarillo, C. R. Carlson, and J. K. Salisbury, "Configuration tracking for continuum manipulators with coupled tendon drive," *IEEE Trans. Robot.*, vol. 25, no. 4, pp. 798–808, Aug. 2009.
- [19] R. J. Webster and B. A. Jones, "Design and kinematic modeling of constant curvature continuum robots: A review," *Int. J. Robot. Res.*, vol. 29, pp. 1661–1683, 2010.
- [20] I. D. Walker, "Continuous backbone "continuum" robot manipulators," *ISRN Robot.*, vol. 2013, 2013, Art. no. 726506.
- [21] N. Simaan, "Snake-like units using flexible backbones and actuation redundancy for enhanced miniaturization," in *Proc. IEEE Int. Conf., Robot. Autom.*, 2005, pp. 3012–3017.
- [22] A. Muller, "Internal preload control of redundantly actuated parallel manipulators-its application to backlash avoiding control," *IEEE Trans. Robot.*, vol. 21, no. 4, pp. 668–677, Aug. 2005.
- [23] D. B. Camarillo, C. F. Milne, C. R. Carlson, M. R. Zinn, and J. K. Salisbury, "Mechanics modeling of tendon-driven continuum manipulators," *IEEE Trans. Robot.*, vol. 24, no. 6, pp. 1262–1273, Dec. 2008.
- [24] A. Trevisani, "Planning of dynamically feasible trajectories for translational, planar, and underconstrained cable-driven robots," *J. Syst. Sci. Complexity*, vol. 26, no. 5, pp. 695–717, 2013.
- [25] D. Lau, D. Oetomo, and S. K. Halgamuge, "Generalized modeling of multilink cable-driven manipulators with arbitrary routing using the cable-routing matrix," *IEEE Trans. Robot.*, vol. 29, no. 5, pp. 1102–1113, Oct. 2013.
- [26] D. Lau, D. Oetomo, and S. K. Halgamuge, "Inverse dynamics of multilink cable-driven manipulators with the consideration of joint interaction forces and moments," *IEEE Trans. Robot.*, vol. 31, no. 2, pp. 479–488, Apr. 2015.
- [27] S. Fang, D. Franitza, M. Torlo, F. Bekes, and M. Hiller, "Motion control of a tendon-based parallel manipulator using optimal tension distribution," *IEEE/ASME Trans. Mechatron.*, vol. 9, no. 3, pp. 561–568, Sep. 2004.
- [28] M. Carricato, "Direct geometrico-static problem of underconstrained cable-driven parallel robots with three cables," *J. Mech. Robot.*, vol. 5, no. 3, 2013, Art. no. 31008.
- [29] Y. Chen, J. H. Chang, A. S. Greenlee, K. C. Cheung, A. H. Slocum, and R. Gupta, "Multi-turn, tension-stiffening catheter navigation system," in *Proc. IEEE Int. Conf., Robot. Autom.*, 2010, pp. 5570–5575.
- [30] I. A. Gravagne, C. D. Rahn, and I. D. Walker, "Large deflection dynamics and control for planar continuum robots," *IEEE/ASME Trans. Mechatron.*, vol. 8, no. 2, pp. 299–307, Jun. 2003.
- [31] W. S. Rone and P. Ben-Tzvi, "Multi-segment continuum robot shape estimation using passive cable displacement," in *Proc. IEEE Int. Symp., Robot. Sensors Environ.*, 2013, pp. 37–42.
- [32] K. Xu and N. Simaan, "An investigation of the intrinsic force sensing capabilities of continuum robots," *IEEE Trans., Robot.*, vol. 24, no. 3, pp. 576–587, Jun. 2008.
- [33] E. Tatlicioglu, I. D. Walker, and D. M. Dawson, "New dynamic models for planar extensible continuum robot manipulators," in *Proc. IEEE/RSJ Int. Conf. Intell. Robots Syst.*, 2007, pp. 1485–1490.
- [34] V. Falkenhahn, T. Mahl, A. Hildebrandt, R. Neumann, and O. Sawodny, "Dynamic modeling of constant curvature continuum robots using the Euler-Lagrange formalism," in *Proc. IEEE/RSJ Int. Conf., Intell. Robots Syst.*, 2014, pp. 2428–2433.
- [35] D. C. Rucker and R. J. Webster, "Statics and dynamics of continuum robots with general tendon routing and external loading," *IEEE Trans. Robot.*, vol. 27, no. 6, pp. 1033–1044, Dec. 2011.
- [36] R. E. Goldman, A. Bajo, and N. Simaan, "Compliant motion control for continuum robots with intrinsic actuation sensing," in *Proc. IEEE Int. Conf., Robot. Autom.*, 2011, pp. 1126–1132.
- [37] B. He, Z. Wang, Q. Li, H. Xie, and R. Shen, "An analytic method for the kinematics and dynamics of a multiple-backbone continuum robot," *Int. J. Adv. Robot. Syst.*, vol. 10, no. 84, pp. 1–13, 2013.
- [38] M. W. Hannan and I. D. Walker, "Kinematics and the implementation of an elephant's trunk manipulator and other continuum style robots," *J. Robot. Syst.*, vol. 20, no. 2, pp. 45–63, 2003.
- [39] K. Xu and N. Simaan, "Analytic formulation for kinematics, statics, and shape restoration of multibackbone continuum robots via elliptic integrals," *J. Mech. Robot.*, vol. 2, no. 1, 2010, Art. no. 11006.
- [40] J. C. Simo and L. Vu-Quoc, "On the dynamics of flexible beams under large overall motions The plane case: Part II," *J. Appl. Mech.*, vol. 53, no. 4, pp. 855–863, 1986.
- [41] M. Rolf and J. J. Steil, "Constant curvature continuum kinematics as fast approximate model for the Bionic Handling Assistant," in *Proc. IEEE/RSJ Int. Conf., Intell. Robots Syst.*, 2012, pp. 3440–3446.
- [42] A. A. Shabana, *Computational Continuum Mechanics*. Cambridge, U.K.: Cambridge Univ. Press, 2011.
- [43] M. W. Spong and M. Vidyasagar, *Robot Dynamics and Control*. Hoboken, NJ, USA: Wiley, 2008.
- [44] M. M. Dalvand, S. Nahavandi, and R. D. Howe, "High speed vision-based 3D reconstruction of continuum robots," in *Proc. IEEE Int. Conf., Syst., Man, Cybern.*, 2016, pp. 618–623.
- [45] J. Jung, R. S. Penning, and M. R. Zinn, "A modeling approach for robotic catheters: effects of nonlinear internal device friction," *Adv. Robot.*, vol. 28, no. 8, pp. 557–572, 2014.



Mohsen Moradi Dalvand received the Doctoral degree in mechanical engineering from Monash University, Melbourne, VIC, Australia.

He is a Research Fellow in Robotics and Haptics with the Institute for Intelligent Systems Research and Innovation (IISRI), Deakin University, Geelong, VIC, Australia. His research interests include robotics and automation with a special focus on surgical robotics and medical instrumentation. He is currently a visiting scholar with the Harvard Paulson School of Engineering and Applied Sciences,

Harvard University, Cambridge, MA, USA. More information about him can be found on his personal website at <https://mohsenmdalvand.com/>.



Saeid Nahavandi received a Ph.D. from Durham University, Durham, U.K., in 1991.

He is an Alfred Deakin Professor, Pro Vice-Chancellor (Defence Technologies), Chair of Engineering, and the Director for the Institute for Intelligent Systems Research and Innovation at Deakin University. He has published more than 750 papers in various international journals and conferences. His research interests include modeling of complex systems, robotics, and haptics.

Dr. Nahavandi is a Fellow of Engineers Australia (FIEAust), the Institution of Engineering and Technology (FIET), and Senior member of IEEE (SMIEEE). He is the Co-Editor-in-Chief of the IEEE SYSTEMS JOURNAL, an Associate Editor for the IEEE/ASME TRANSACTIONS ON MECHATRONICS, an Associate Editor for the IEEE TRANSACTIONS ON SYSTEMS, MAN AND CYBERNETICS: SYSTEMS, and an IEEE Access Editorial Board member.



Robert D. Howe received the Bachelor's degree in physics from Reed College, Portland, OR, USA, and the Doctoral degree in mechanical engineering from Stanford University, Stanford, CA, USA.

He worked in the electronics industry in Silicon Valley. After receiving the Ph.D. degree, he joined the faculty at Harvard in 1990. He is currently the Abbott and James Lawrence Professor of Engineering with the Harvard Paulson School of Engineering and Applied Sciences. He directs the Harvard BioRobotics Laboratory, which investigates the roles of sensing

and mechanical design in motor control, both in humans and robots. His research interests focus on manipulation, the sense of touch, and robot-assisted and image-guided surgery.

Dr. Howe is a Fellow of the AIMBE